Energy 232 (2021) 121037

Contents lists available at ScienceDirect

Energy

journal homepage: www.elsevier.com/locate/energy

Investigation of two hybrid aircraft propulsion and powering systems using alternative fuels

Shaimaa Seyam*, Ibrahim Dincer, Martin Agelin-Chaab

Department of Mechanical and Manufacturing Engineering, Ontario Tech University, Oshawa, Ontario, Canada

ARTICLE INFO

Article history:
Received 1 February 2021
Received in revised form
16 May 2021
Accepted 21 May 2021
Available online 27 May 2021

Keywords:
Molten carbonate fuel cell
Solid oxide fuel cell
Fuels
Energy
Exergy
Efficiency
Aircrafts

ABSTRACT

Sustainable aviation attracts the attention of academic and industrial research with the aim of lowering the environmental impact and reducing greenhouse gas emissions. This paper presents two proposed high bypass three-shaft turbofan engines combined a molten carbonate fuel cell (MCFC-turbofan) and a solid oxide fuel cell (SOFC-Turbofan). Energy and exergy analyses are conducted to investigate the performance of the aircraft at the cruising operation mode. The used fuels are kerosene and an alternative fuel blend of 75% methane and 25% hydrogen. The results show that the base turbofan has a maximum thrust force of 153 kN, while the SOFC- and MCFC-turbofans have 116 kN and 107 kN, respectively. The thermal and exergy efficiencies are 43.4% and 52% for the base-turbofan, 52.8% and 66.2% for the SOFC-turbofan, and 71% and 87.6% for the MCFC-turbofan. The carbon emissions are reduced from 18 kg/s to about 3.7 kg/s using the alternative fuel blends. The turbofan engine weight increases by 18% using the SOFC and 40% using the MCFC, while the thrust-to-weight-ratio is reduced from 2.7 for the base-turbofan, to 1.5 for the SOFC-turbofan, and 1.06 for the MCFC-turbofan. Adding a fuel cell increases the engine weight but also improves the system performance and reduces the emissions.

1. Introduction

Aviation is an essential link to connect countries globally and therefore plays a vital role in the economic activities of the world. The number of passenger and freight flights has significantly increased over the years due to globalization. This rapid growth rate increased the carbon emissions seven-times to 1034 Tg CO_2/yr [1]. Focusing on Canada, the energy use of aviation transportation in Canada has increased from 180 to 300 PJ between 1990 and 2019 [2]. This energy use relies on aviation turbo fuels, which are kerosene-based fuels. Consequently, the greenhouse gas (GHG) emissions have increased substantially from 15 to 22 Mt of CO_2e [3,4], which contributes about 2% of total GHG emissions from all transportation sectors in Canada.

Several studies have been conducted on clean aviation transportation. For example, Kousoulidou and Lonza [5] collected data from actual flight information EUROCONTROL and Eurostat statistics for European flights to predict the consumption of biokerosene, and conventional kerosene and their impact on carbon emission. They discovered that the total fuel consumption was obtained to be about 170 million tonnes resulting in 400 million tonnes of CO_2 emissions by 2030, and the main contribution to these data is the conventional fuels. Therefore, the European Union planned for the use of biofuels such as clustered hydroprocessed esters and fatty acids (HEFA), hydrotreated vegetable oils (HVOs) and biomass-to-liquid (BTL) biojet fuels in order to reduce global CO_2 emissions from the aviation sector. Also, Schripp et al. [6] analyzed the use of ternary alternative jet fuel blends in a real aircraft, the A300-600 aircraft with the PW4158 engine. The first fuel blend is a mixture of Jet A-1, 30%vol HEFA, and 8%vol alcohol-to-jet (ATJ), and the second blend is Jet A-1, HEFA, ATJ, and synthesized iso-paraffins (SIP). Thus, the soot formation significantly decreased, and the particle emissions reduced by 29%–37% according to the flight conditions.

Moreover, adding hydrogen (20%v/v) to kerosene in a scramjet has improved the performance of kerosene supersonic combustion under 3.8 Mach number inlet conditions. The heat released is intensified resulting in higher exit temperature and pressure and more OH radical at low-temperature conditions. This is because the hydrogen addition promotes the pre-evaporation and combustion

* Corresponding author.
E-mail addresses: shaimaa.seyam@ontariotechu.net (S. Seyam), Ibrahim.dincer@uoit.ca (I. Dincer), Martin.Agelin-Chaab@uoit.ca (M. Agelin-Chaab).

https://doi.org/10.1016/j.energy.2021.121037
0360-5442/

Nomenclature

Symbols

A	Area [cm^2]
ex	Specific exergy [kJ/kg]
$\dot{E}x$	Exergy rate [kW]
F	Faraday constant [C/mol]
F/A	Fuel-to-air mass ratio [kg_f/kg_a]
g	Gibbs function [kJ/kmol]
h	Specific enthalpy [kJ/kg]
j	Current density [mA/cm^2]
m	Mass flow rate [kg/s]
M	Mach number [-]
N	Number of cells [-]
P	Pressure [kPa]
$\dot{Q}$	Heat rate [kW]
R	Resistive losses [$\Omega.cm^2$]
$\dot{R}$	Molar gas constant [J/mol.K]
s	Specific entropy [kJ/kg.K]
S/C	Steam-to-carbon ratio [kg_w/kg_f]
T	Temperature [K]
T/W	Thrust-to-weight ratio [-]
U	Air speed [m/s]
V	Voltage [V]
VOC	Voltage operating current [AV]
$\dot{W}$	Power [kW]
Z	Altitude [km]

Greek letters

η	Thermal efficiency [%] /loss voltage [V]
ψ	Exergy efficiency [%]
Γ	Thrust force [kN]
ν	Fuller diffusion volume coefficient [-]
ξ	inverter efficiency [%]
α	charge transfer coefficient [-]
γ	Specific heat ratio [-]

Abbreviations

AC	Alternative current
BPR	Bypass ratio
BR	Catalytic burner
CC	Combustion chamber
DC	Direct current
EN	Exit hot nozzle
GT	Gas turbine
FC	Fuel cell
FN	Fan nozzle
HP	High pressure
IP	Intermediate
LP	Low pressure
SOFC	Solid oxide fuel cell
MCFC	Molten carbonate fuel cell
TIT	Turbine inlet temperature
TE	Turbine Exit
TSFC	Thrust specific fuel consumption

Subscript

a	Ambient
e	Exit flow
elec	electric
eng	engine
i	Inlet flow
in	Inlet heat or work
loss	loss
o	Outlet flow
out	Outlet heat or work

heat release and CO oxidation [7]. Furthermore, Badami et al. [8] conducted a small-size turbojet performance using a traditional Jet-A with two alternative fuels, such as synthetic gas to liquid and a blended biofuel of Jet-A and Jatropha Methyl Ester. A similar performance was achieved despite the lower heat value for alternative fuels. However, the unburned hydrocarbon emissions were reduced by 25%–35% using alternative fuels.

Alternative fuels such as hydrogen and methane have been investigated to test the ability to use them in aircraft engines. Hydrogen is a carbon-free fuel with a high heating value and high energy carrier but has less volume. Methane has a low carbon intensity rating, which can significantly reduce carbon emissions. Adding hydrogen to methane or other hydrocarbon fuels has been tested experimentally. Hydrogen can decrease the ignition delay and increase laminar burning velocities [9]. A mixture of ammonia, methane, and hydrogen has also been conducted experimentally in a high-pressure combustion test rig for gas turbines. The mixture can achieve high stability flame with low emissions at a low equivalence ratio [10]. Bicer and Dincer [11] performed a life cycle assessment of a well-to-wake approach for conventional and alternative aircraft fuels, such as hydrogen, ammonia, methanol, ethanol, and liquified natural gas. They showed that hydrogen and liquified natural gas have the lowest environmental impact compared to other fuels because of the clean and renewable fuel production.

Fuel cells are introduced into aircraft engines as powering systems to increase engine performance. They have been used in land transportation [12,13] however, few studies have combined fuel cells with aircraft engines. For example, Ji et al. [14] compared thermodynamically three configurations of turbojet engines using kerosene fuel. The configurations are two-shaft turbojet, two-shaft turbojet with afterburner, two-shaft turbojet with a solid oxide fuel cell (SOFC) and afterburner. The last design has achieved the best thermal efficiency between 36% and 42% according to different turbine inlet temperatures from 1550 K to 1700 K and a pressure ratio of 24. Besides, Waters and Cadou [15] presented three aircraft engines of unmanned aerial vehicle combined with SOFC and catalytic partial oxidation reactors to reduce fuel burn. The engines are turbojet, high bypass ratio and low bypass ratio of turbofans. The fuel used in the system is JP-5. They found that fuel efficiency increased by about 8% for 90 kW high bypass turbofan with a modest cost.

Moreover, Ji et al. [16] conducted their study on unmanned aerial vehicles. They proposed the concept of turbine-less jet engines combined with SOFC and battery to operate the fuel cell. The proposed design showed better performance than a traditional turbojet engine with a maximum pressure ratio of 33 and a Mach number of 0.3. Also, Bakalis et al. [17] studied a hybrid SOFC-GT and conducted an optimization to achieve the best performance in the whole operating range. The optimized hybrid system can produce a net power of 246.4 kW (192.2 kW for SOFC and 57.2 kW for GT) with 58.5% thermal efficiency.

Note that aircraft manufacturers are concerned about the extra weight that affect the aerodynamic performance of airplanes due to

changing fuel types and engine systems. However, studies have proven the opposite. Verstraete [18] investigated the utilization of hydrogen fuel in the aviation sector. It was found that hydrogen storage capacity can be performed in a smaller span and wing area. The gross weight of the hydrogen-fueled aircraft is less by 30% relative to that of a kerosene-fueled engine, which reduces the direct operating costs from 6.65 to 6.53 ¢/seat. In addition, the improvements in engine specific fuel consumption were 20% fewer sensitives for a hydrogen-fueled than that of kerosene-fueled aircraft. Also, the ratio of operating empty weight between the hydrogen-fueled to kerosene-fueled engines is 95.9%. Further, the lift/drag ratio of the airplane is less by 15.3% for hydrogen fuel. However, the energy utilization was higher for the hydrogen fuel of 643.4 kJ/seat than that of kerosene fuel by 68%.

The Government of Canada declared a plan to strictly reduce the emissions from all transportation sectors, including aviation by 2030 [19]. In order to implement this plan, the current paper should consider innovative powering systems and alternative fuels. As mentioned earlier, few studies were focused on hybrid SOFC turbojet engines for military and surveillance and performed thermodynamic analysis but did not include exergy analysis. Therefore, there is a need to extend the research area to include other types of fuel cells combined with other aircraft engines, in order to provide unique solutions for sustainable aviation transportation.

The main objective of this paper is to study two proposed hybrid turbofan engines using the SOFC and MCFC. The paper conducts thermodynamic analyses of the two hybrid turbofan engines and compares their performance with the traditional turbofan engine using an alternative fuel blend of 75% methane and 25% hydrogen and a traditional kerosene-based fuel. In addition, the effect of fuel cells on the thrust force, specific thrust fuel consumption, total engine weight, and emissions is investigated.

Table 1
Specification of turbofan aircraft engine.

Specifications	Turbofan [20]		
Aircraft engine	Rolls-Royce Trent 1000		
General Characteristics:			
Type	Three-spool high-bypass turbofan		
Dimension	Length: 4.738 m, diameter: 2.85 m (fan)		
Dry weight	5936–6120 kg		
Components			
Compressors	One-stage LP (fan), 8-stage IP, 6-stage HP compressor		
Combustors	Single annular combustor with 18-off fuel spray nozzles		
Turbines	Single-stage HP (13,391 RPM), single-stage IP turbine (8937 rpm), and 6-stage LP turbine (2683 rpm)		
Air bleeding	2% after the HP compressor and before the combustors.		
Performance:			
Overall pressure ratio	50:1	SFC take-off	479.16 kg/(h.kN)
TIT	1800 K	Air mass flow	1090–1210 kg/s
Thrust take-off	265.3–360.4 kN	BPR	>10:1

TIT: Turbine inlet temperature, SFC: Specific fuel consumption, BPR: Bypass ratio.

2. System description

The proposed aviation systems are two turbofan engines using different fuel cells and an alternative fuel mixture consisting of 75% methane and 25% hydrogen to improve system performance and reduce emissions. The baseline system is a turbofan aircraft, as shown in Fig. 1, which comprises three spools; the 1-stage fan with

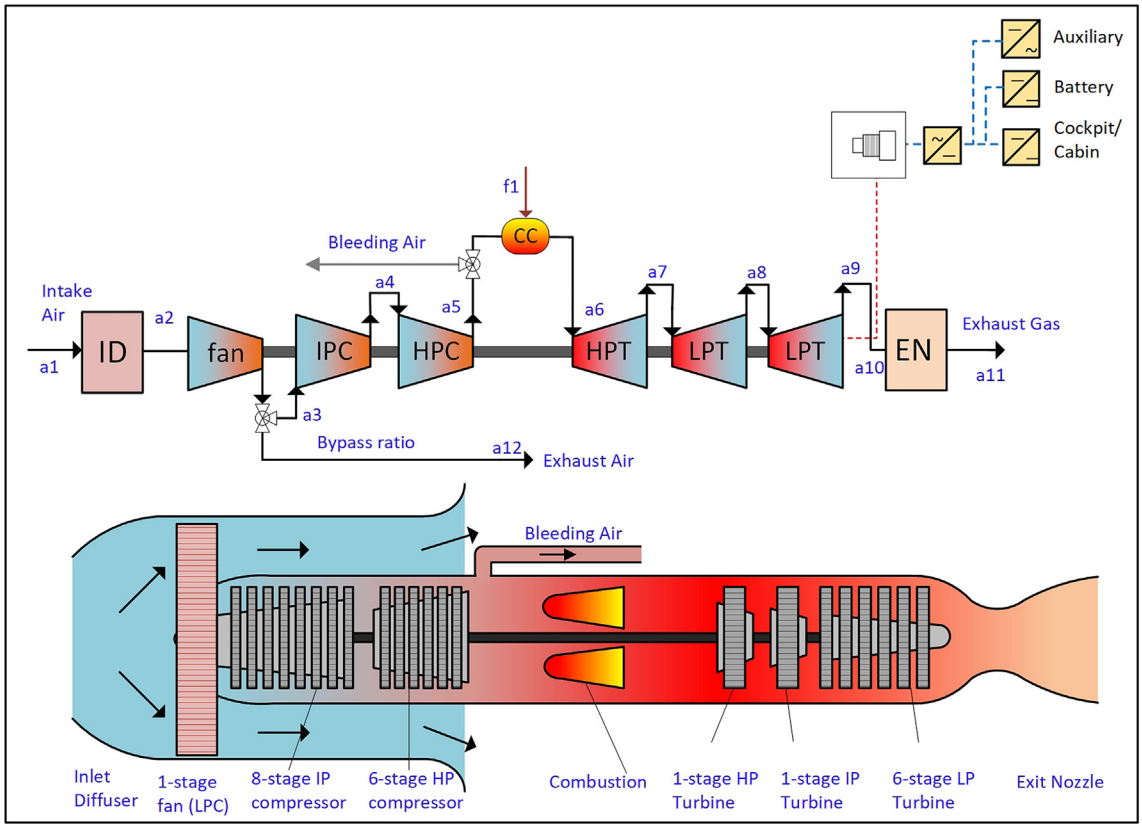

Fig. 1. The configuration of the aviation base (A-Base) system.

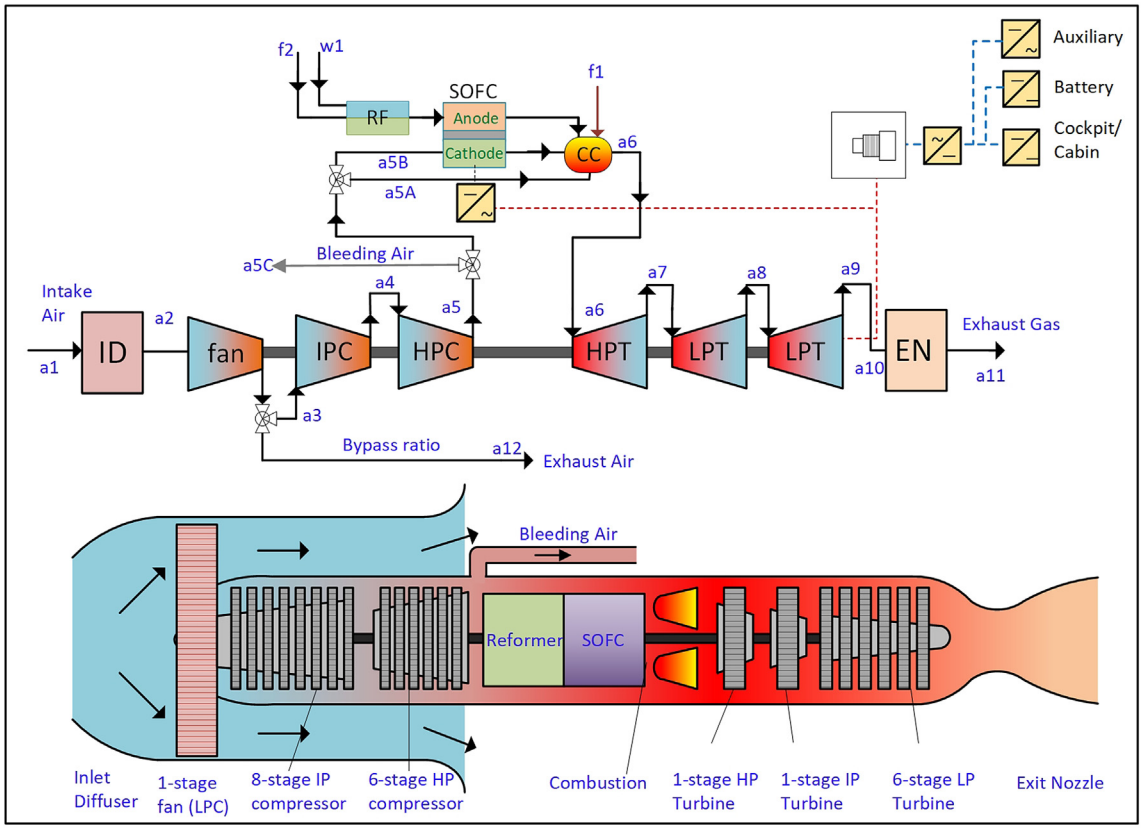

Fig. 2. Hybrid SOFC-turbofan engine.

a 6-stage LP turbine, the 8-stage IP compressor with 1-stage IP turbine, and the 6-stage HP compressor with a 1-stage HP turbine. The fuel used in the aviation system is kerosene with a chemical formula of $C_{10}H_{22}$. The power generated from the gas turbine (GT) system is used to operate the cockpit of the airplane, and auxiliary systems, and battery for storage and emergency cases. A turbofan aircraft engine is running Boeing 787 Dreamline in Air Canada. The specifications of the turbofan are listed in Table 1.

2.1. Hybrid SOFC-turbofan engine

The hybrid SOFC turbofan consists of a turbofan aircraft engine with a high bypass ratio (high-BPR) and a SOFC, as shown in Fig. 2. The airflow enters the diffuser. Some of the air is bypassed around the GT tell the high-pressure compressors to the atmosphere, while the remaining air flows through the GT. The compressed air from the IPC and HPC compressors flows through the cathode of SOFC and the combustion chambers. The fuel blend and the steam enter the reformer and the anode of SOFC. The exit flows from the SOFC burn with the compressed air in the combustion chamber. The exhaust gases flow through the HP turbine, then the LP turbine and the exit hot nozzle.

2.2. Hybrid MCFC-turbofan engine

The hybrid MCFC turbofan engine consists of a turbojet aircraft engine with an MCFC and a catalytic burner or an oxidizer, as shown in Fig. 3. The air flows through the GT, and a portion of exhaust gas flows from the MCFC to the afterburner. The fuel blend with the steam injection enters the anode of the MCFC. The catalytic burner receives the exhaust gases to oxidize the fuels and produce carbon dioxides. The exhaust from the catalytic burner enters the cathode of MCFC that chemically react with the electrolyte to produce clean exhaust gases. If any carbon dioxide or monoxide exits as byproducts in the exhaust gases, then the exhaust gas returns to the burner and re-oxidizes into the cathode of the MCFC. The clean exhaust gas leaves the GT through the hot exit nozzle.

3. Methodology

The thermodynamic analysis is conducted to investigate the performance of the hybrid turbofan engines. The following subsections explain the modeling of turbofan engines, MCFC, and SOFC.

3.1. Thermodynamic analysis

The thermodynamic analysis is governed by the first and second law of thermodynamics and compare the developed system to the ideal case. The software used for the analyses are the EES (Engineering Equation solver) and Aspen-Plus software because of their reliable thermodynamic properties as well as the calculation methods. They have been excessively used by researchers for thermodynamic analyses for several systems.

The general form of the energy balance equation in steady-state can be expressed as follows [21]:

$$\sum_{in}\dot{Q}_{cv}+\sum_{in}\dot{W}_{cv}+\sum_{i}\dot{m}_i\left(h_i+\frac{1}{2}U_i^2+gZ_i\right) = \sum_{out}\dot{Q}_{cv}+\sum_{out}\dot{W}_{cv}+\sum_{e}\dot{m}_e\left(h_e+\frac{1}{2}U_e^2+gZ_e\right) \quad (1)$$

where $\dot{Q}_{cv}$ and $\dot{W}_{cv}$ represent the heat transfer and the work

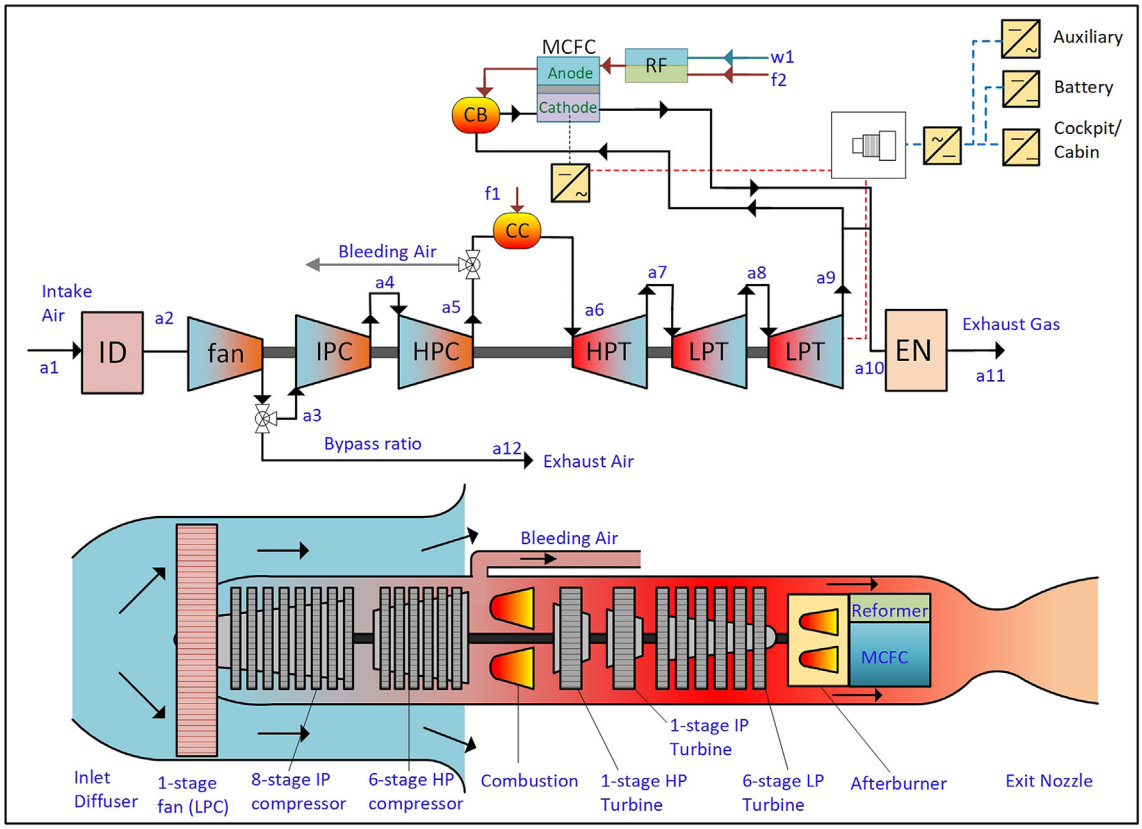

Fig. 3. Hybrid MCFC-turbofan engine.

crossing the boundaries of a closed system of each component. The steady energy flow is expressed as $(h + U^2/2 + gZ)$, which represents the internal energy of the media, the specific kinetic energy, and the specific potential energy, respectively. h is the specific enthalpy, U is the stream velocity of the working fluid, g is the gravitational acceleration, and Z is the elevation from the reference point.

The general form of the second law of thermodynamics can be represented by the exergy balance equation in a steady-state condition for each process. It can be written as follows [21]:

$$\sum_i \dot{m}_i ex_i + \sum_{in} \dot{E}x_Q + \sum_{in} \dot{E}x_W + \sum_{in} \dot{E}x_{KE} = \sum_e \dot{m}_e ex_e + \sum_{out} \dot{E}x_Q + \sum_{out} \dot{E}x_W + \sum_{out} \dot{E}x_{KE} + \dot{E}x_D \quad (2)$$

where $\dot{E}x_D$ refers to the exergy destruction rate, $\dot{E}x_W$ denotes the exergy work done or required by the process, $\dot{E}x_{KE}$ is the kinetic exergy, and $\dot{E}x_Q$ is thermal exergy due to the heat transfer within the boundaries $(\dot{Q}_{cv,i})$ and depends on the reference temperature T_o. They can be defined as the following [21]:

$$\dot{E}x_{KE} = \dot{m}U^2 \Big/ 2 \quad (3a)$$

$$\dot{E}x_W = \dot{W}_{cv} \quad (3b)$$

$$\dot{E}x_{Q,i} = \left(1 - \frac{T_o}{T_{s,i}}\right)\dot{Q}_{cv,i} \quad (3c)$$

The specific exergy of each stream is comprised of specific physical exergy, $ex_{ph,i}$, and specific chemical exergy, $ex_{ch,i}$, and are described as follows [21]:

$$\overline{ex}_i = \overline{ex}_{ph,i} + \overline{ex}_{ch,i} = \sum_i \left[\left(\overline{h}_i - \overline{h}_o\right) - T_o\left(\overline{s}_i - \overline{s}_o\right) \right] + \sum_i n_i \left(\overline{g}_f^o + \overline{g}_{T_o} - \overline{g}^o\right) \quad (4)$$

The physical specific exergy depends on the specific enthalpy and entropy for a substance at a specific temperature and pressure, while the chemical exergy depends on the chemical changes of a component composition during the chemical reactions. It depends on the Gibbs function of a unit mole of a substance $\overline{g}$, which consists of the Gibbs function of formation of each substance $\overline{g}_f^o$, Gibbs function of a substance at a specific temperature $\overline{g}_{T_o}$, and Gibbs function at a reference temperature $\overline{g}^o$.

3.2. Modeling of a turbofan engine

The ambient condition varies according to the altitude (Z), and both of them decrease with increasing the altitude. The ambient temperature T_a and ambient pressure P_a are described below [22]:

$$T_a = 288.15 + L_a Z \quad (5a)$$

$$P_a = 101.325\left(\frac{288.15}{T_a}\right)^{\frac{g}{R_a L_a}} \quad (5b)$$

Where L_a is the base temperature lapse rate per kilometre of

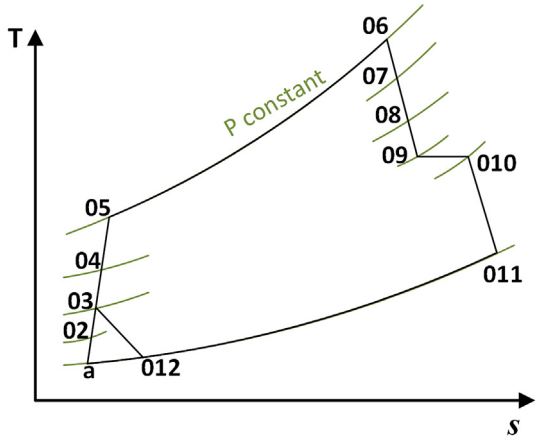

Fig. 4. T-s diagram for base-turbofan engine.

geopotential altitude and equals to −6.5 K/km, g is the gravitational acceleration, R_a is the gas constant of air in J/kg.K. The flight speed is defined as $U_a = M\sqrt{\gamma R_a T_a}$, where M is a Mach number, γ is the specific heat ratio of air (1.4). The inlet air temperature to the diffuser is described as [22]:

$$T_{02} = T_a\left(1 + \frac{\gamma - 1}{2}M^2\right) \tag{6a}$$

$$P_{02} = P_a\left(1 + \frac{\gamma - 1}{2}M^2\right)^{\frac{\gamma}{\gamma-1}} \tag{6b}$$

The T-s diagram is graphed in Fig. 4 for the base-turbofan. The energy balance and exergy balance equations for the components in the turbofan engine are shown in Table 2. The isentropic efficiencies are 90% for turbines and compressors and 87% for hot and fan nozzles. The percentage total pressure drops in the combustion chamber relative to HPC is 2% [23], and the percentage pressure losses in the jet pipe relative to LPT is 20% [23].

The hot nozzle and fan nozzle should be checked for chocking pressure, which is estimated as the following equation [22]:

$$\frac{P_i}{P_C} = \frac{1}{\left[1 - \left(\frac{1}{\eta}\right)\left(\frac{\gamma-1}{\gamma+1}\right)\right]^{\frac{\gamma}{\gamma-1}}} \tag{12}$$

If the ratio of nozzle inlet pressure P_i to the ambient pressure $P_a$is greater than P_i/P_C, then the nozzle is choking. Therefore, the nozzle exit pressure, temperature, and speed are calculated as the following equations [22]:

$$P_e = \frac{P_i}{P_i/P_C} \tag{13a}$$

$$T_e = T_i\frac{2}{\gamma + 1} \tag{13b}$$

$$U_e = \sqrt{\gamma R_a T_e} \tag{13c}$$

The net power of the gas turbine is determined to be [21,22]:

$$\dot{W}_{GT} = \Sigma\dot{W}_T - \Sigma\dot{W}_C \tag{14}$$

The thrust force of the turbofan is defined as in Eq. (15). The total thrust force is the summation of the fan thrust force from the exit fan nozzle at state point 11 and the hot thrust force from the exit nozzle at state point 12 [22].

$$\Gamma = \sum_k \dot{m}_{e,k}U_{e,k} - \sum_k \dot{m}_{e,k}U_{e,k} - \sum_k A_{e,k}(P_{e,k} - P_a) \tag{15}$$

The thrust specific fuel consumption (TSFC) is determined as [22].

$$\mathrm{TSFC} = \frac{\dot{m}_f}{\Gamma} \tag{16}$$

The energetic and exergetic efficiencies of turbofan are described by Ref. [22].

$$\eta_{GT} = \frac{\dot{W}_{GT} + \Gamma U_a}{\dot{Q}_{CC}} \tag{17a}$$

Table 2
The energy and exergy balance equations for basic components in turbofan engines [22].

Components	Energy balance		Exergy balance	
Inlet Diffuser	$\dot{m}_{i,d}\left(h_{i,d} + \frac{U_a^2}{2}\right) = \dot{m}_{e,d}\left(h_{e,d} + \frac{U_{02}^2}{2}\right)$	(7a)	$\dot{m}_{i,d}ex_{i,d} + \dot{m}_{i,d}\frac{U_a^2}{2} = \dot{m}_{e,d}ex_{e,d} + \dot{m}_{e,d}\frac{U_{02}^2}{2} + \dot{E}x_{D,d}$	(7b)
Compressors	$\dot{W}_c = \dot{m}_c(h_{e,c} - h_{i,c})/\eta_c$	(8a)	$\dot{m}_{i,c}ex_{i,c} + \dot{W}_c = \dot{m}_{e,c}ex_{e,c} + \dot{E}x_{D,c}$	(8b)
Turbines	$\dot{W}_t = \eta_t\dot{m}_t(h_{i,t} - h_{e,t})$	(9a)	$\dot{m}_{i,t}ex_{i,t} = \dot{W}_t + \dot{m}_{e,t}ex_{e,t} + \dot{E}x_{D,t}$	(9b)
Exit Nozzle	$\dot{m}_{i,n}\left(h_{i,n} + \frac{U_s^2}{2}\right) = \dot{m}_{e,n}\left(h_{e,n} + \frac{U_n^2}{2}\right)$	(10a)	$\dot{m}_{i,n}ex_{i,n} + \dot{m}_{i,n}\frac{U_s^2}{2} = \dot{m}_{e,n}ex_{e,n} + \dot{m}_{e,n}\frac{U_n^2}{2} + \dot{E}x_{D,n}$	(10b)
Reactors	$\sum_R \dot{m}_{in,R}h_{in,R} + \dot{Q}_{i,r} = \sum_P \dot{m}_{e,P}h_{e,P}$	(11a)	$\sum_R \dot{m}_{i,R}ex_{i,R} + (T_o/T_s - 1)\dot{Q}_{i,r} = \sum_P \dot{m}_{e,P}ex_{e,P} + \dot{E}x_{D,r}$	(11b)

Table 3
Specifications of alternative fuels for turbofan engines.

Specifications	Hydrogen [24]	Methane [25]	Kerosene [26]
Molecular formula	H_2	CH_4	$C_{12}H_{24}$
Molecular weight, M_i [kg/kmol]	2.016	16.043	142
Adiabatic flame temperature [°C]	2000	1963	2093
Auto-ignition temperature [°C]	571	537	640
Density at 40 °C [kg/m^3]	0.0773	0.657	760–810
Viscosity at 40 °C [mm^2/s]	109	18.72	1–1.9
High heating value [MJ/kg]	141.9	55.5	46.2
Low heating value [MJ/kg]	119.0	50	43.0

Table 4
The specifications of MCFC [31].

Parameters	MCFC
Operating pressure [bar]	2
Operating temperature [K]	923
Current density, j [mA/cm^2]	150
Active cell area, A_{cell} [cm^2]	900
N_{cell} in one stack	100 cells
Anode activation energy, $\Delta\bar{h}_{an}$ [J/mol]	53,500
Cathode activation energy, $\Delta\bar{h}_{ca}$ [J/mol]	77,300

$$\psi_{GT} = \frac{\dot{W}_{GT} + \Gamma U_a}{\dot{E}x^{Q}_{CC}} \tag{17b}$$

Note that aviation fuel is kerosene-based fuel. Therefore, the current paper uses kerosene with a chemical formula of $C_{12}H_{24}$. A fuel mixture of methane and hydrogen has a mass fraction of 75% and 25%, respectively. The fuel specifications are listed in Table 3. The stoichiometric reactions for the kerosene, methane, and hydrogen are listed below:

- Kerosene: $C_{12}H_{24} + 18\ O_2 \rightarrow 12\ CO_2 + 12H_2O$ $(\Delta\bar{h}^0_{298K} = -7674.5$ kJ/mol)
- Hydrogen: $2H_2 + O_2 \rightarrow 2H_2O$ $(\Delta\bar{h}^0_{298K} = -286$ kJ/mol)
- Methane: $CH_4 + 2\ O_2 \rightarrow CO_2 + 2H_2O$ $(\Delta\bar{h}^0_{298K} = -891$ kJ/mol)

3.3. Modeling of molten carbonate fuel cell

The MCFC uses molten salt electrolytes whose materials are eutectic mixtures of Li_2CO_3, Na_2CO_3, and K_2CO_3, which have been widely adopted [27]. The specifications of the MCFC are listed in Table 4. The carbonates melt at approximately 500 °C, and the molten carbonates transfer ions. A stable operating temperature should be at 923 K (650 °C) to prevent electrolyte solidification or volatilization. An MCFC produces electricity by the electrochemical reactions. The steam reforming (SR) and water gas shift (WGS) reactions sequentially occur to produce H_2 and CO in the MCFC stack [28]. The reforming reaction is a highly intensive endothermic process, since it removes the heat by the hydrogen oxidation. Other reactions may occur, such as Boudouard reaction, CO hydrogenation, and methanation at the anode; and polycarbonate, peroxide, and superoxide at the cathode [27]. After the electrochemical reactions, the anode emits the unreacted fuel and byproducts, such as CO_2 and water, while the cathode emits excess air. The CO_2 is consumed to form molten carbonates. Any unreacted fuels flow to the catalytic burner to be combusted with air, and its exhaust of carbon, and oxygen gas flows to the cathode.

- SR: $CH_4 + H_2O \rightarrow CO + 3H_2$ $(\Delta\bar{h}^0_{298K} = 206$ kJ/mol)
- WGS: $CO + H_2O \rightarrow CO_2 + H_2$ $(\Delta\bar{h}^0_{298K} = -41$ kJ/mol)
- Anode: $H_2 + CO_3^{2-} \leftrightarrow CO_2 + H_2O + 2e^-$
  $CO + CO_3^{2-} \leftrightarrow 2\ CO_2 + 2e^-$
- Cathode: $0.5\ O_2 + CO_2 + 2e^- \leftrightarrow CO_3^{2-}$
- Overall: $H_2 + 0.5\ O_2 + CO_2 \leftrightarrow H_2O + CO_2$ $(\Delta\bar{h}^0_{298K} = -242$ kJ/mol)

The cell voltage is calculated by considering the Nernst loss, activation polarization, and concentration loss [29]. The cell voltage V_{cell} of the MCFC can be expressed by:

$$V_{MCFC,cell} = -\frac{\Delta\bar{g}}{2F} - \frac{\bar{R}T}{2F}\ln\left(\frac{P_{H_2O,an}P_{CO_2,an}}{P_{H_2,an}\sqrt{P_{O_2,ca}}P_{CO_2,ca}}\right) - j(R_{an} + R_{ca} + R_{ohm}) \tag{18}$$

where the first part of Eq. (18) is the reversible potential at standard conditions (E^0), and the second part is the Nernst loss. Both the first and second parts are the total Nernst potential, which is the maximum potential achieved through the electrochemical reaction. When the current is zero, the Nernst potential becomes the open-circuit voltage. $\bar{R}$ and F are the molar gas constant (8.314 J/mol.K) and Faraday constant (96,485 C/mol), $\Delta\bar{g}$ is the Gibbs free energy, can be expressed as $\Delta\bar{g} = 0.002474\,T^2 + 48.996T - 243730$, T is the MCFC stack temperature in K, j, is the current density in mA/cm^2. R_{an}, R_{ca}, and R_{ohm} represent the activation losses of the anode and cathode, and ohmic loss [Ω.cm^2], respectively, and P is the partial pressure at each electrode. The activation polarization losses happen when breaking the chemical bonds of O_2 and H_2 molecules in the electrochemical reaction [30]. The R_{an} and R_{ca} can be expressed as [29]:

$$R_{an} = 2.27 \times 10^{-5} \times \exp\left(\frac{\Delta\bar{h}_{an}}{\bar{R}T}\right) \times P_{H_2}^{-0.42}P_{CO_2}^{-0.17}P_{H_2O}^{-1.0} \tag{19}$$

$$R_{ca} = 7.505 \times 10^{-6} \times \exp\left(\frac{\Delta\bar{h}_{ca}}{\bar{R}T}\right) \times P_{O_2}^{-0.43}P_{CO_2}^{-0.09} \tag{20}$$

where $\Delta\bar{h}_{an}$ and $\Delta\bar{h}_{ca}$ are the activation energy in the anode and cathode, respectively. The ohmic loss happens because of ionic and electronic conduction at the electrodes and contacts. It is called the internal resistance and is calculated by the following Arrhenius equation [29]:

$$R_{ohm} = 0.5 \times \exp\left[3016\left(\frac{1}{T} - \frac{1}{923}\right)\right] \tag{21}$$

Table 5
The specifications of SOFC [35].

Parameter	SOFC
Operating pressure [kPa]	200
Operating temperature [K]	1123
Current density, j [mA/cm^2]	500
Active cell area, A_{cell} [cm^2]	900
N_{cell} in one stack	100 cells
Anode thickness, δ_{an} [m]	5.0×10^{-4}
Cathode thickness, δ_{ca} [m]	5.0×10^{-5}
Electrolyte thickness, δ_{el} [m]	1.0×10^{-5}
Interconnect thickness, δ_{in} [m]	1.0×10^{-5}
Pre-exponential coefficient for anode, γ_{an} [A/m^2]	7.0×10^{9}
Pre-exponential coefficient for cathode, γ_{ca} [A/m^2]	2.9×10^{9}
Anode activation energy, $E_{act,an}$ [J/mol]	120,000
Cathode activation energy, $E_{act,ca}$[J/mol]	120,000
Pore diameter for anode and cathode, r [m]	5.0×10^{-7}
Porosity of anode, ϵ_{ca} [%]	0.5
Porosity of cathode, ϵ_{ca} [%]	0.5
Tortuosity for anode and cathode, ξ [-]	6
Fuller diffusion volume coefficient for hydrogen, ν_{H2} [-]	7.07
Fuller diffusion volume coefficient for steam, ν_{H_2O} [-]	12.7
Fuller diffusion volume coefficient for oxygen, ν_{O2} [-]	16.6
Fuller diffusion volume coefficient for nitrogen, ν_{N2} [-]	17.9

3.4. Modeling of solid oxide fuel cell

The fuel mixture is mixed with steam and flows to the SOFC anode. The air is flowing to SOFC cathode. The oxygen molecules diffuse to the triple phase boundary to receive the electrons and produce oxygen ions O^{2-}, which are move to the anode to produce electric current. The oxygen is released from the cathode to exit the fuel cell. The oxygen ions react with the hydrogen to produce water on the anode side. The specifications of SOFC is listed in Table 5. The electrochemical reactions of the SOFC are listed below:

- SR: $CH_4 + H_2O \rightarrow CO + 3H_2$ $(\Delta\bar{h}^0_{298K} = 206$ kJ/mol)
- WGS: $CO + H_2O \rightarrow CO_2 + H_2$ $(\Delta\bar{h}^0_{298K} = -41$ kJ/mol)
- Anode: $H_2 + O^{2-} \rightarrow H_2O + 2e^-$
- Cathode: $0.5\ O_2 + 2e^- \leftrightarrow O^{2-}$
- Overall: $H_2 + 0.5\ O_2 \leftrightarrow H_2O$

The cell voltage of SOFC is expressed as the Nernst potential subtracting the activation losses (η_{act}), the concentration losses (η_{con}), and ohmic losses (η_{ohm}), as shown in Eq. (22) [27].

$$V_{SOFC,cell} = -\frac{\Delta\bar{g}}{2F} - \frac{\bar{R}T}{2F}\ln\left(\frac{P_{H_2O,an}}{P_{H_2,an}\sqrt{P_{O_2,ca}}}\right) - \eta_{act} - \eta_{con} - \eta_{ohm} \tag{22}$$

The activation polarization is produced to overcome the reaction energy barriers between electrode and electrolyte, which are solved using the Butler-Volmer Equation [27,32]. The activation losses occurred on the anode ($\eta_{act,an}$) and cathode ($\eta_{act,ca}$) as shown in Eq. (23), where α_{an} and α_{ca} are the charge transfer coefficients of anode and cathode, respectively.

$$\eta_{act} = \eta_{act,an} + \eta_{act,ca} = \frac{\bar{R}T}{2\alpha_{an}F}\sinh^{-1}\left(\frac{j}{2j_{0,an}}\right) + \frac{\bar{R}T}{2\alpha_{ca}F}\sinh^{-1}\left(\frac{j}{2j_{0,ca}}\right) \tag{23}$$

Here, $j_{0,an}$ and $j_{0,ca}$ are the electrode exchange current densities for the anode and cathode, respectively. They are expressed using the Arrhenius' law function of the partial pressure of the reacting species in Eqs. (24) and (25) [33]. The γ_{an} and γ_{ca} are the pre-exponential factors, and $E_{act,an}$ and $E_{act,ca}$ are the activation energy for the electrode reactions, and $P_{ref}$is the reference atmospheric pressure [33].

$$j_{0,an} = \gamma_{an}\left(\frac{P_{H_2}}{P_{ref}}\right)\left(\frac{P_{H_2O}}{P_{ref}}\right)\exp\left(-\frac{E_{act,an}}{\bar{R}T}\right) \tag{24}$$

$$j_{0,ca} = \gamma_{ca}\left(\frac{P_{O_2}}{P_{ref}}\right)^{0.25}\exp\left(-\frac{E_{act,ca}}{\bar{R}T}\right) \tag{25}$$

The ohmic loss is calculated as Eq. (26) considering four resistances to the flow of ions and electrons inside the anode ($\rho_{an}\delta_{an}$), cathode ($\rho_{ca}\delta_{ca}$), electrolyte ($\rho_{el}\delta_{el}$), and interconnections ($\rho_{in}\delta_{in}$). They are a function of specific material resistivity ρ and the component thickness δ for planar SOFC [33].

$$\eta_{ohm} = j(\rho_{an}\delta_{an} + \rho_{ca}\delta_{ca} + \rho_{el}\delta_{el} + \rho_{in}\delta_{in}) \tag{26}$$

The concentration losses are the voltage drop caused by the mass transfer of the gas phase into and through the electrode [33]. They are given by the following equations for the anode and cathode:

$$\eta_{con,an} = -\frac{\bar{R}T}{2F}\ln\left(1 - \frac{j}{j_{L,an}}\right) + \frac{\bar{R}T}{2F}\ln\left(1 + \frac{P_{H_2}j}{P_{H_2O}j_{L,an}}\right) \tag{27}$$

$$\eta_{con,ca} = -\frac{\bar{R}T}{2F}\ln\left(1 - \frac{j}{j_{L,ca}}\right) \tag{28}$$

The limiting current densities are defined for the anode and cathode as follow:

$$j_{L,an} = \frac{2FP_{H_2}D_{an(\text{eff})}}{\bar{R}T} \tag{29a}$$

$$j_{L,ca} = \frac{2FP_{O_2}D_{ca(\text{eff})}}{\bar{R}T} \tag{29b}$$

where the $D_{an,\text{eff}}$ and $D_{ca,\text{eff}}$ are the effective diffusivities of reactant species through the porous anode and cathode, respectively. The ordinary diffusion coefficient of each gas is evaluated using Eq. (30) and converted into an effective value using Eq. (31) by considering the porosity and the tortuosity of the electrode pores.

$$D_{O,ik} = \frac{1 \times 10^{-7} T^{1.25} \left(M_i^{-1} + M_k^{-1}\right)^{0.5}}{P\left(\nu_i^{1/3} + \nu_k^{1/3}\right)} \tag{30}$$

$$D_{O,i(eff)} = D_{O,i}\left(\frac{\varepsilon}{\xi}\right) \tag{31}$$

Where ν is the Fuller diffusion volume coefficient of each gas [34]. ε and ξ are the porosity and tortuosity of anode or cathode. The i and k refers to the mixture H_2 and H_2O used for anode and O_2 and N_2 mixture for the cathode. The Knudsen diffusion coefficients were calculated and converted into the effective values as the following

$$D_{K,i} = 97r\sqrt{\frac{T}{M_i}} \tag{32a}$$

$$D_{K,i(eff)} = D_{K,i}\left(\frac{\varepsilon}{\xi}\right) \tag{32b}$$

The overall diffusion coefficient was calculated harmonically averaging the Knudsen effective diffusion coefficient and the ordinary effective diffusion coefficient as described below:

$$\frac{1}{D_{i(\text{eff})}} = \frac{1}{D_{K,i(\text{eff})}} + \frac{1}{D_{O,i(\text{eff})}} \tag{33}$$

Therefore, the effective diffusivities of anode and cathode are described below:

$$D_{an(\text{eff})} = \left(\frac{P_{H_2O}}{P_{an}}\right) D_{H_2(\text{eff})} + \left(\frac{P_{H_2}}{P_{an}}\right) D_{H_2O(\text{eff})} \tag{34a}$$

$$D_{ca(\text{eff})} = D_{O_2(\text{eff})} \tag{34b}$$

The resultant power output of a fuel cell (FC) is presented as follows:

$$\dot{W}_{FC,AC} = jA_{\text{cell}} V_{\text{cell}} N_{\text{cell}} \xi_{DC-AC} \tag{35}$$

where A_{cell} is the total active area of a fuel cell in cm^2, N_{cell} is the number of cells, ξ_{DC-AC} is the inverter efficiency from direct current (DC) to alternating current (AC) and is equivalent to 0.95. The electric efficiency of a fuel cell can be determined as Eq. (36a), while the thermal energetic and exergetic efficiencies can be evaluated as Eq. (36b and c). The added heat of fuel cell, $\dot{Q}_{FC,add}$, is considered as the summation of added heat through the anode, cathode, and the catalytic burner.

$$\eta_{FC,e} = \frac{\dot{W}_{FC,AC}}{\dot{W}_{FC,AC} + \dot{W}_{MCFC,loss}} \tag{36a}$$

$$\eta_{FC,th} = \frac{\dot{W}_{FC,AC}}{\dot{Q}_{FC,add}} \tag{36b}$$

$$\psi_{FC,th} = \frac{\dot{W}_{FC,AC}}{\dot{E}x^{Q}_{FC,add}} \tag{36c}$$

The performance of the developed turbofan systems can be determined as the overall energetic efficiency η_{eng}, and the overall exergetic efficiency ψ_{eng}, as follows:

$$\eta_{eng} = \frac{\dot{W}_{FC} + \dot{W}_{GT} + \Gamma U_a}{\dot{Q}_{CC} + \dot{Q}_{FC} + \dot{Q}_{SR} + \dot{Q}_{WGS}} \tag{37}$$

$$\psi_{eng} = \frac{\dot{W}_{FC} + \dot{W}_{GT} + \Gamma U_a}{\dot{E}x^{Q}_{CC} + \dot{E}x^{Q}_{FC} + \dot{E}x^{Q}_{SR} + \dot{E}x^{Q}_{WSG}} \tag{38}$$

4. Results and discussion

The turbofan engine is modeled using the Aspen Plus considering the specifications of the turbofan Rolls-Royce Trent 1000, as shown in Table 1. The equation of state is chosen to be Soave-Redlick-Kwong (SRK) for thermodynamic properties because it is most-widely accepted equation for modern chemical processes and recommended for gas mixture and electrolytes (such as carbonate electrolyte CO_3^{2-}) at high temperature and pressure conditions [36–38]. The turbofan is modeled using isentropic compressors and turbines and an expansion valve for modeling the nozzle. The separate stoichiometric reactions are used for SOFC, MCFC anode and cathode, WGS, SR, and afterburner. In addition, a split unit (SEP) is added to split the carbonate CO_3^{2-} to be recirculated to the anode.

The turbofan has an overall pressure of 50 kPa and a bypass ratio of 10:1. The inlet mass flow rate to the fan is selected to be 1210 kg/s. The airplane is assumed to be in cruising condition at 10 km altitude, in which the ambient conditions are 293.2 K and 26.4 kPa. The Mach number at this altitude for Boeing 747 Dreamline is 0.83. There are three Aspen Plus models for three turbofan system, as shown in Fig. 5. The thermodynamic results are listed in Table 6 for the base-turbofan engine. Also, the power and heat for components are listed in Table 7. As a result, the inlet air speed, U_a, is 248.6 m/s, and the exit speed and conditions for the exit fan at a state point of 12 and exhaust nozzle at a state point of 11 are listed in Table 8.

The pressure compression ratio for the fan, IPC, and HPC are 1.4, 5.98, and 5.98, respectively. Also, the pressure ratio of HPT, IPT, and LPT are 0.4, 0.55, and 0.4, respectively, for the base-turbofan engine. However, for the SOFC turbofan, the pressure ratio of HPT, IPT, and LPT are 0.35, 0.35, and 0.29 and for MCFC turbofan are 0.385, 0.5, 0.3, respectively, in order to maintain the exhaust temperature at LPT entry of 1100 K. The choking pressure ratio was checked at the exit nozzles, which are 2.046 and 2.105 for the hot nozzle and fan nozzle, respectively. However, the inlet to exit pressure ratio is higher for both nozzles, meaning that the thrust force counts for both speed and pressure difference between inlet and exit air. This change in pressure is a result of the fuel mass flow rate at F1 for all systems. As shown in Fig. 6, the kerosene mass flow rate is about 6 kg/s, while the mass flow rates for 75% methane and 25% hydrogen are 1.7 and 1.9 kg/s for the SOFC- and MCFC-turbofan, respectively. The fuel-to-air mass ratios (F/A) are 0.055, 0.0175, and 0.0177 kg_f/kg_a for the base-, SOFC-, and MCFC-turbofans, respectively, due to the constant values of inlet air flow rate and the excess oxygen (20%) for all systems. The main reason for reducing the fuel mass is the higher low and high heating values for the alternative fuel blend (67 and 77 MJ/kg) compared to that of kerosene (43 and 46 MJ/kg), respectively.

The change in pressure for the inlet and exit as well as the change in speed significantly affects the thrust force of the turbofan engines, as shown in Fig. 7. The maximum thrust force is observed to be 153 kN for base-turbofan using kerosene fuel because of the higher exit hot speed and pressure, as shown in Table 8. The thrust force of the SOFC- and MCFC-turbofans are 116 and 107 kN, respectively. The thrust specific fuel consumption (TSFC) are 0.039,

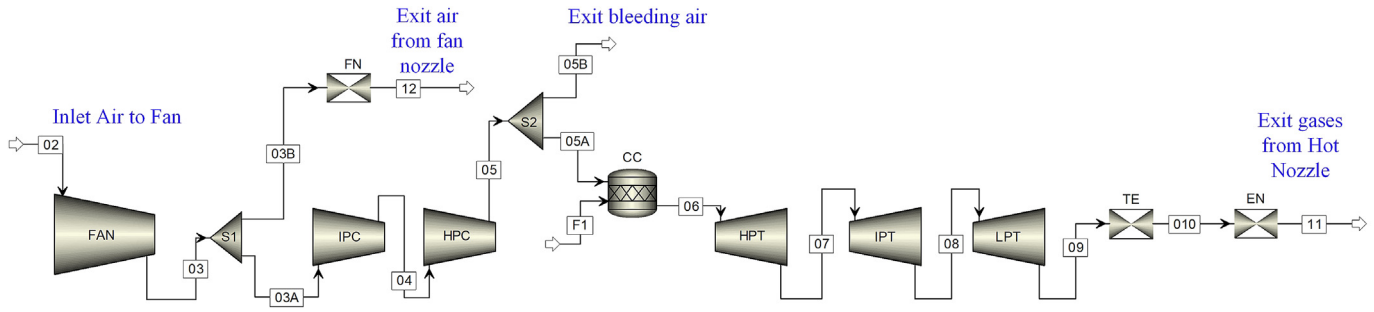

(a) Base-turbofan system

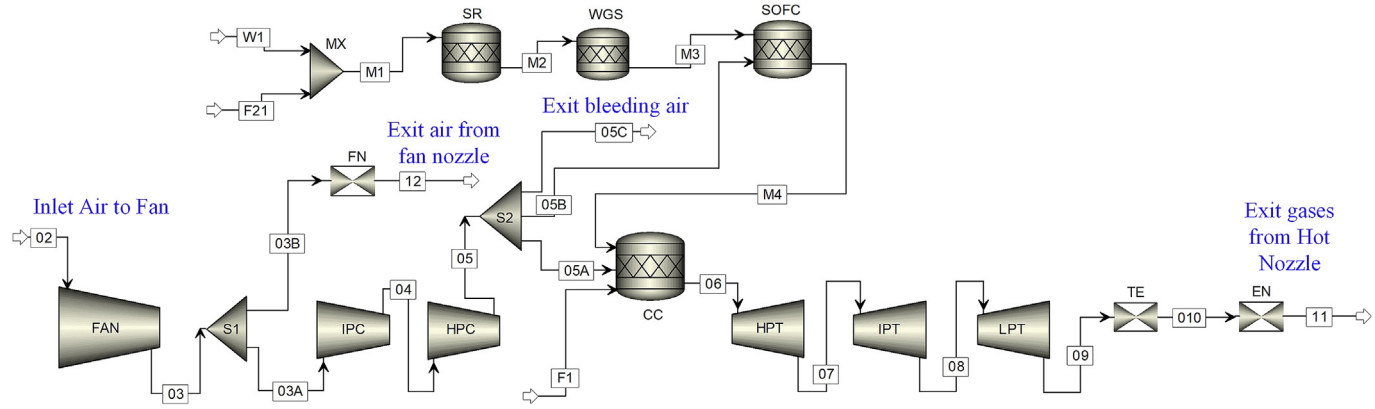

(b) SOFC-turbofan system

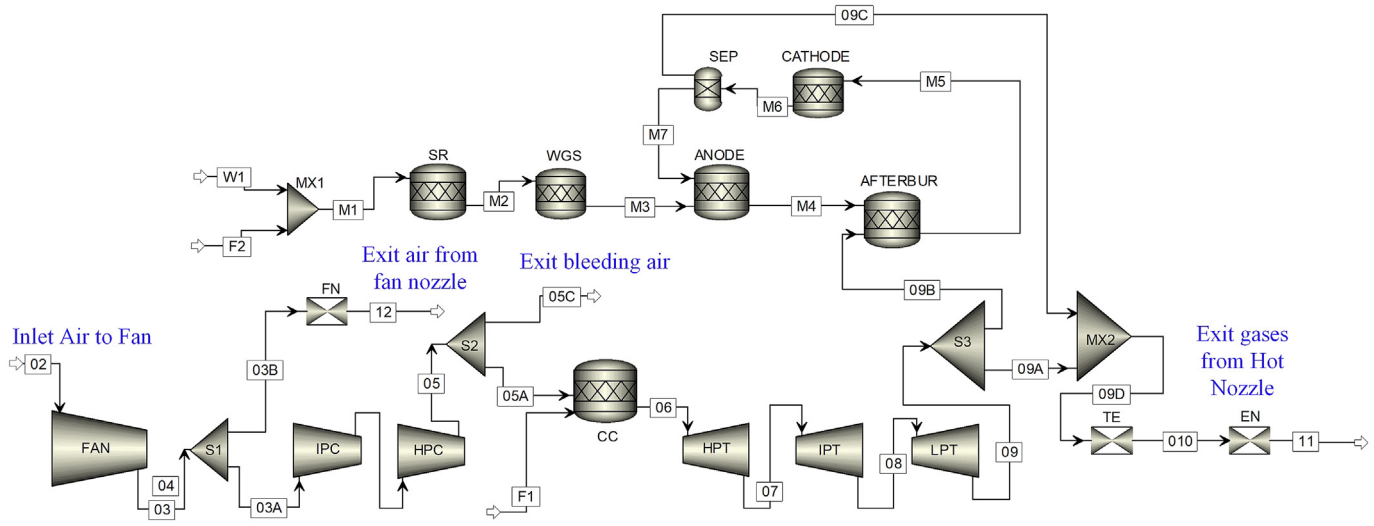

(c) MCFC-turbofan system

Fig. 5. Aspen flow chart for base and hybrid turbofan systems.

0.015, and 0.018 kg/(s.kN) for the base-, SOFC-, and MCFC-turbofan engines, respectively. The thrust force due to the fan is about 40% of the total thrust using fuel cells and 50% of the total thrust for the base-turbofan.

Adding an extra powering system adds more weight to the airplane. Fig. 8 shows the weight of engines, including the fuel cells for the SOFC and MCFC. The weight of the turbofan is about 6000 kg (58.9 kN). The weight of the SOFC and MCFC are 17 kN and 42.5 kN, respectively. The increase in total engine weight will decrease the thrust-to-weight (T/W) ratio from 2.61 for the base-turbofan to 1.53 for the SOFC-turbofan and 1.06 for the MCFC-turbofan.

The net power and added heat are estimated for the three turbofan engines, as shown in Fig. 9. The base-turbofan has the highest net power, and the thrust energy is the major contributor to it. For the base-turbofan, the total net power is 47.3 MW, and the added heat is 109 MW. The fuel cells provide about 950 kW, and the net power of the gas turbine system only is a minimum of 3.3 MW for the SOFC-turbofan, while the maximum gas turbine net power

Table 6
Thermodynamic results of the base-turbofan system.

#	$\dot{m}$ [kg/s]	T [K]	P [kPa]	h [kJ/kg]	s [kJ/kg.K]	ex_{ph} [kJ/kg]	ex_{ch} [kJ/kg]	$\dot{E}x$ [kW]
2	1210.0	253.9	40.7	−44.80	0.2505	−74.61	4.48	−84856.6
3	1210.0	279.8	57.0	−18.73	0.2514	−48.81	4.48	−53645.7
03A	110.1	279.8	57.0	−18.73	0.2514	−48.81	4.48	−4881.8
03B	1099.9	279.8	57.0	−18.73	0.2514	−48.81	4.48	−48763.9
4	110.1	484.7	340.7	189.99	0.2954	146.79	4.48	16655.7
5	110.1	818.8	2037.6	549.13	0.3401	492.59	4.48	54732.2
05A	107.9	818.8	2037.6	549.13	0.3401	492.59	4.48	53637.5
05B	2.2	818.8	2037.6	549.13	0.3401	492.59	4.48	1094.6
6	113.9	1800.0	2000.0	−548.87	1.3662	1511.33	61.70	179129.3
7	113.9	1515.5	800.0	−940.97	1.3953	1110.57	61.70	133492.6
8	113.9	1350.6	440.0	−1162.92	1.4137	883.14	61.70	107593.6
9	113.9	1127.5	176.0	−1455.28	1.4428	582.08	61.70	73310.8
10	113.9	1127.5	171.0	−1455.28	1.4512	579.59	61.70	73027.2
11	113.9	1127.5	83.6	−1455.28	1.6585	517.76	61.70	65986.5
12	1099.9	279.7	27.1	−18.73	0.4657	−112.69	4.48	−119028.7
F1	6.0	293.2	200.0	−2124.03	−7.5357	0.25	47772.49	285107.7

Table 7
The thermodynamic results of components in the base-turbofan engine.

Components	$\dot{Q}$ [kW]	$\dot{W}$ [kW]	$\dot{E}x_D$ [kW]	η [%]	ψ [%]
FAN	0	31547.2	336.3	99	98.9
HPC	0	39545.6	1469.1	90	96.3
HPT	0	44650.2	986.5	90	97.8
IPC	0	22981.5	1444.1	90	93.7
IPT	0	25274.8	624.3	90	97.6
LPT	0	33293.4	989.4	90	97.1
EN	0	0	7040.7	87	90.4
FN	0	0	70264.7	87	41.0
TE	0	0	283.6	98	99.6
CC	109082.6	0	250639.3	42.5	41.7

is 9.2 MW for the base-turbofan.

The exergy destruction rates for the major components are graphed in Fig. 10. The total exergy destruction rate is 334 MW for the base-turbofan, 233 MW for the SOFC-turbofan, and 168 MW for the MCFC-turbofan. The combustion and nozzles are major contributors to the total exergy destruction because of the chemical reactions and large temperature difference compared to the standard conditions. This reflects the energy and exergy efficiency of the systems as shown in Fig. 11. The base-turbofan has the minimum thermal and exergetic efficiency of 43.4 and 52%, respectively. The SOFC-turbofan has 52.8% and 66.2% for energetic and exergetic efficiencies, respectively. The MCFC-turbofan shows the maximum performance of 71% energetic efficiency and 87.6% exergetic efficiency.

The SOFC and MCFC results are compared, as shown in Table 9. In order to maintain high electric efficiency, the operating current density is 500 mA/cm^2 for the SOFC and 150 mA/cm^2 for MCFC. However, the cell area is the same as 900 cm^2. This results in the voltage operating current of 349.1 VA for the SOFC and 110.7 VA for

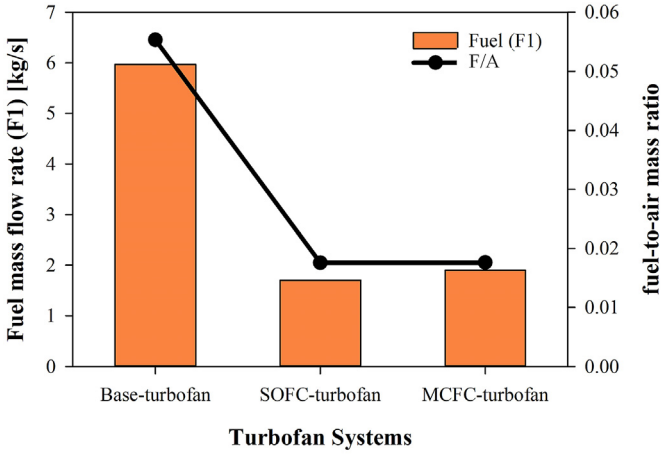

Fig. 6. The fuel mass flow rate and the fuel-to-air ratio of turbofan systems.

the MCFC. To produce high power about 950 kW, many stacks are required. For example, the number of stacks is 28 for the SOFC and 70 for the MCFC. The weight of one cell is 620 g, which is equivalent to 62 kg for 100 cells [39]. That means the total weight of the SOFC and MCFC are 1736 kg and 4340 kg, respectively, which is 2.5 times the weight of SOFC, while the current density of SOFC is 3.3 times that of the MCFC. The heat of chemical reactions is 2928 kW for the SOFC and 4003 kW for the MCFC, leading to higher thermal and exergetic efficiencies for the SOFC than that of the MCFC. Regarding the environmental impact, the base-turbofan using kerosene produces about fourfold the amount using a fuel mixture of 75% methane and 25% hydrogen. Also, the exhaust gases emit the same amount of CO_2 since there is no reduction units. Using alternative

Table 8
The exit conditions for turbofan systems.

Parameters	Units	Base-Turbofan	SOFC-Turbofan	MCFC-Turbofan
Exit hot speed, U_{11}	m/s	607.8	501.6	533.9
Exit hot pressure, P_{11}	kPa	83.6	42.0	51.2
Exit hot temperature, T_{11}	K	967.8	768	870
Exhaust mass flow rate at #11	kg/s	1099.9	109.9	109.6
Exit fan speed, U_{12}	m/s	306.1	306.1	306.1
Exit fan pressure, P_{12}	kPa	27.1	27.1	27.1
Exit fan temperature, T_{12}	K	279.8	279.8	279.8
Air mass flow rate at #12	kg/s	1099.9	1099.9	1099.9

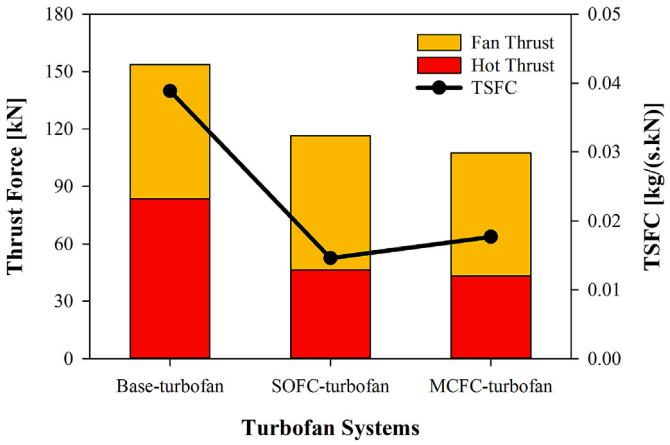

Fig. 7. The Thrust force and TSFC of turbofan systems.

fuel reduces the carbon emissions to a fifth of the value, and using a fuel cell drops the emissions by about 7.5% for the SOFC and MCFC, as shown in Table 10.

The effect of the current density of fuel cells is studied. The current density varies from 100 to 600 mA/cm^2. The power of the SOFC and MCFC are oscillating with increasing current density, as

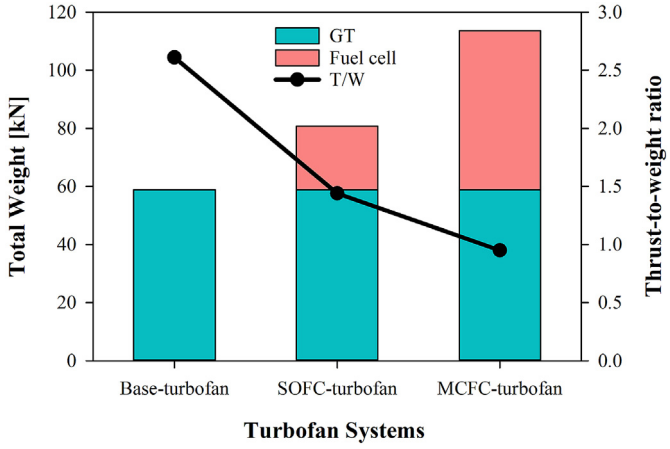

Fig. 8. The total weight of turbofan systems and its thrust-to-weight ratio.

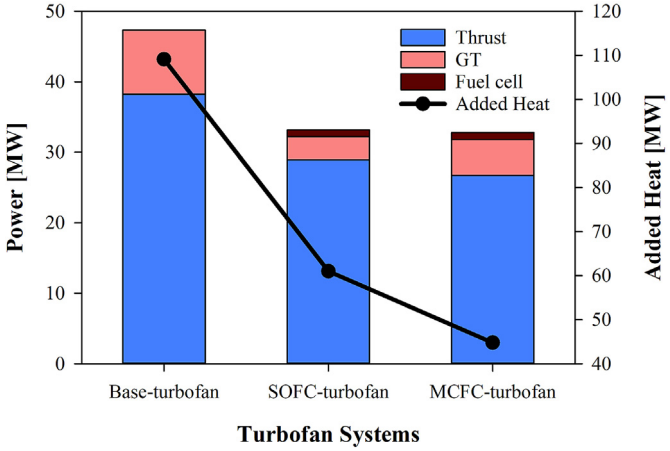

Fig. 9. The net power and added heat of turbofan systems.

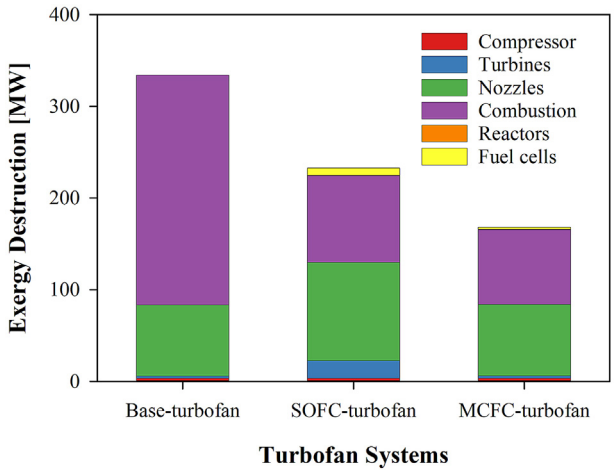

Fig. 10. The exergy destruction of the components in turbofan engines.

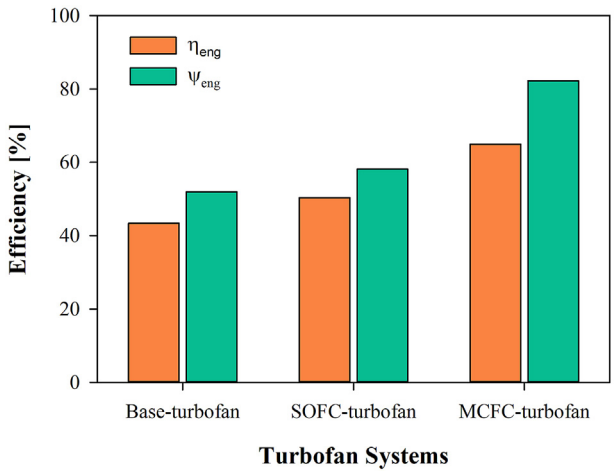

Fig. 11. The thermal and exergy efficiency of fuel cells and turbofan systems.

Table 9
Comparison of SOFC and MCFC results.

Parameters	Units	SOFC	MCFC
Operation current density	mA/cm^2	500	150
Cell area	cm^2	900	900
Number of cells in one stack	–	100	100
Number of stacks	–	28	70
Fuel cell weight	kg	1736	4340
VOC	VA	349.1	110.7
Cell voltage	V	0.776	0.820
Total loss voltage	V	0.173	0.222
$\dot{W}_{net}$	kW	977.5	946.6
$\dot{Q}_{add}$	kW	2928	4003
η_{elec}	%	81.7	78.5
η	%	33.4	23.6
ψ	%	45.4	34.7

Table 10
The CO_2 emissions for turbofan engines.

System	Produced CO_2 [kg/s]	Exhaust CO_2 [kg/s]	Reduction percentage
Base-Turbofan	18.46	18.46	0.00%
SOFC-turbofan	4.00	3.70	7.41%
MCFC-turbofan	4.06	3.75	7.51%

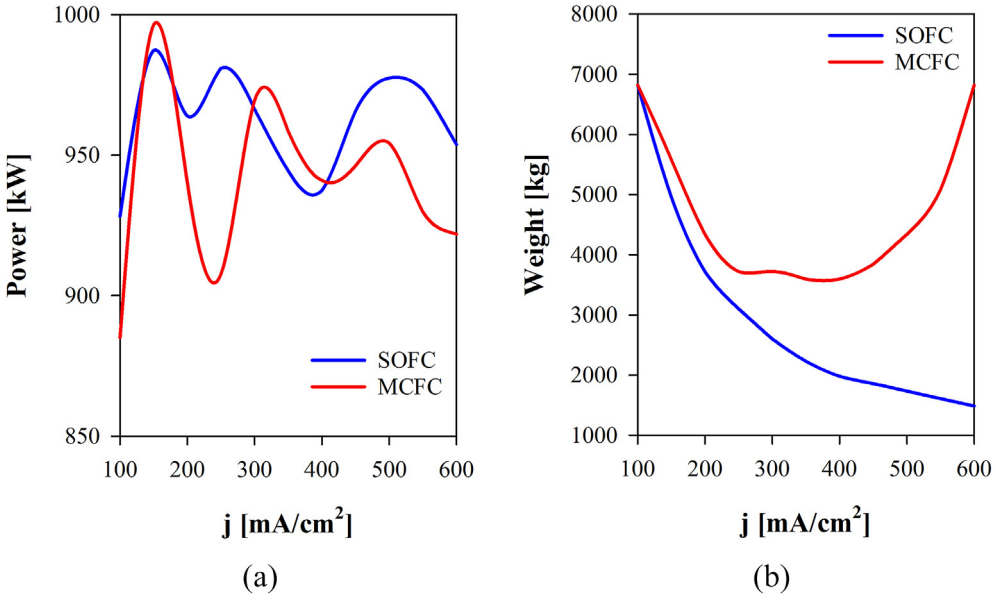

Fig. 12. The effect of current density on fuel cell power (a) and weight (b).

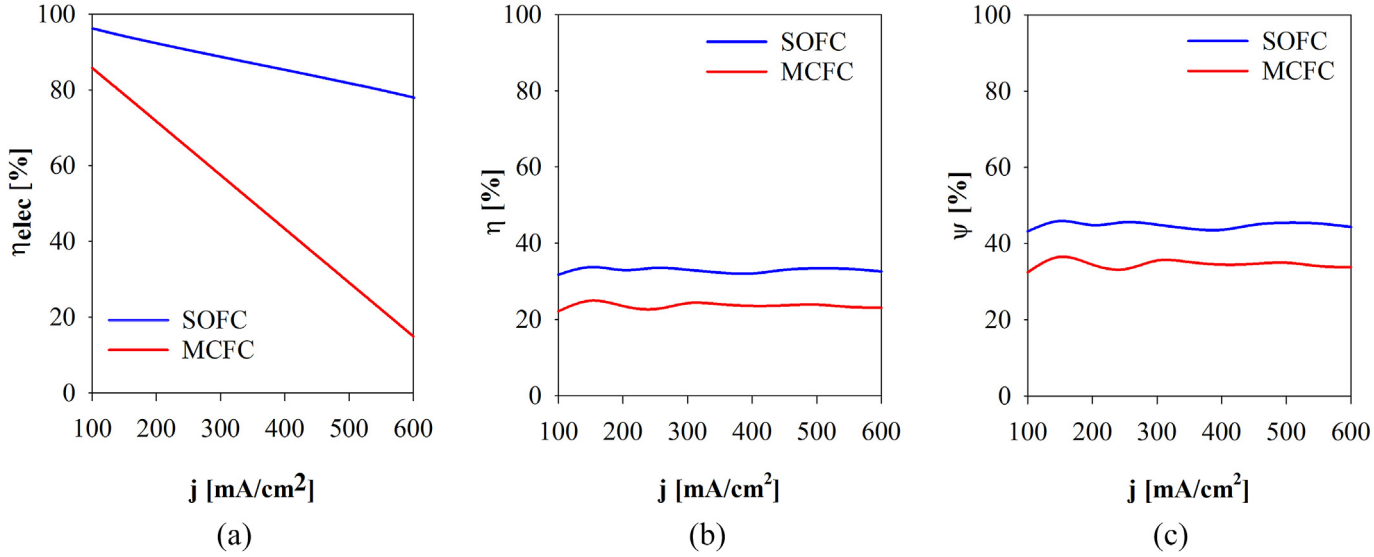

Fig. 13. The effect of current density on electric efficiency (a), thermal efficiency (b), and exergy efficiency (c).

shown in Fig. 12-a, but the SOFC power is more than the MCFC power for most conditions except at 150 and 300–400 mA/cm^2. The maximum number of stacks is 110 cells with 900 cm^2 of cell area to ensure equal cell distribution in the airplane. The weight of one stack is 64 kg, as the minimum cell weight is 640 g/cell. Fig. 12-b shows the decrease of the SOFC weight with increasing current density. However, the MCFC weight has almost a parabolic shape where the maximum weight is 6800 kg at 100 and 600 mA/cm^2 and the minimum weight is at 3800 kg for the range of 250–450 mA/cm^2.

In addition, the current density of fuel cell is investigated on the efficiencies, as shown in Fig. 13. The increasing current density of the SOFC and the MCFC decreases the electric efficiency from 96% to 82% and from 86 to 18%, respectively. The thermal efficiency of the SOFC and the MCFC almost remains constant over the increase of current density, which is about 36% and 26%, respectively. Also, the exergetic efficiencies of the SOFC and MCFC are about 45% and 35% for the SOFC and MCFC, respectively.

The current hybrid turbofans are compared with other hybrid propulsion systems, as shown in Table 11, at the cruising conditions and altitude 10 km and more. There are few studies focused on SOFC hybrid propulsion systems. Waters and Cadou [15] investigated different types of hybrid UAV using L-BPR and H-BPR turbofan and turbojet combining with SOFC and catalytic partial oxidation (COPx). The fuel was JP-5 which is a mixed fuel of hydrogen, aromatic, and sulfur. The TSFC and Γ vary from 0.012 to 0.026 kg/(s.kN) and 3.95–5.3 kN, respectively. The proposed systems increased the fuel efficiency by 4–8% and the overall performance increased by 6–15% compared to the baseline engine. In addition, Ji et al. [40] studied a L-BPR turbine-less turbofan of an UAV combined with a SOFC and battery using propane fuel. The TSFC and Γ are 15.85 kg/(s.kN) and 4 kN. The overall efficiency is

Table 11
Comparison of other systems in previous literature at cruising conditions.

Refs.	Aircraft type	Engine type	Fuel	Fuel cell type	Conditions	TSFC [kg/(s.kN)]	Γ [kN]	η_{eng} [%]
Waters and Cadou [15]	UAV	L-BPR turbofan	JP-5	SOFC, CPOx	Z = 16.5 km M = 0.5 $\dot{m}_a$ = 7.26 kg/s $\dot{m}_f$ = 0.078 kg/s	0.021	5.3	NM
	UAV	H-BPR turbofan	JP-5	SOFC, CPOx	Z = 16.5 km M = 0.5 $\dot{m}_a$ = 16.24 kg/s $\dot{m}_f$ = 0.078 kg/s	0.012	3.95	NM
	UAV	Turbojet	JP-5	SOFC, CPOx	Z = 16.5 km M = 0.5 $\dot{m}_a$ = 5.58 kg/s $\dot{m}_f$ = 0.078 kg/s	0.026	5.29	NM
Ji et al. [40]	UAV	L-BPR Turbofan (turbine-less)	Propane	Battery, SOFC	Z = 16.8 km M = 0.5 $\dot{m}_a$ = 7.26 kg/s $\dot{m}_f$ = 0.061 kg/s	15.85	4	59
Ji et al. [35]	UAV	Turbojet (turbine-less)	Propane	SOFC, steam injection	Z = 23.6 km M = 3.5–5 $\dot{m}_a$, $\dot{m}_f$ NM W/A = 0.031 ER = 39	0.89	1.123[a] kN/(kg/s)	54
Current paper	Boeing 787	L-BPR Turbofan	F1	SOFC	Z = 10 km M = 0.83 $\dot{m}_a$ = 1210 kg/s $\dot{m}_f$ = 1.7 kg/s	0.015	116	53
	Boeing 787	L-BPR Turbofan	F1	MCFC	Z = 10 km M = 0.83 $\dot{m}_a$ = 1210 kg/s $\dot{m}_f$ = 1.9 kg/s	0.018	107	71

UAV = unmanned aerial vehicle, NM = not mentioned, CPOx = catalytic partial oxidation, ER = equivalence ratio, W/A = water-to-air ratio, F1 = 75%wt CH_4 + 25% wt H_2, JP-5 = 13.4% wt H_2+ 25% v/v aromatic+ 0.20%wt sulfur.
[a] Specific thrust.

59%. Ji et al. [35] also performed a study on a turbine-less turbojet of an UAV combined with SOFC and steam injection. The TSFC was 0.89 kg/(s.kN), while the specific thrust was 1.123 kN/(kg/s), resulting in an overall thermal efficiency of 54%.

The comparison shows that the previous studies have higher TSFC values compared to that of the present work (0.015 and 0.018 kg/(s.kN)). However, the thrust forces of the current paper are much higher about 116 kN and 107 kN. That is because the previous literatures have focused on a small size surveillance aviation with small air mass flow rate. Also, the overall efficiency of the current hybrid turbofan has a value of 53% for the SOFC, which is slightly less than in the literature but 71% for the MCFC, which is higher than previously reported. This confirms the novelty of the present work, which employs other types of fuel cells such as the SOFC and MCFC with better performance. Nevertheless, there are some limitations of the present research including focusing on one flight phase such as cruising conditions, and neglecting take-off, climb, descent, and landing.

5. Conclusion

Air transportation contributes significantly to GHG emissions. Like many countries around the world, Canada's action plan is to produce more efficient and sustainable aircraft engines by using advanced powering systems and alternative fuels. The current paper thermodynamically investigates high bypass three-shaft turbofan engine of the Rolls Royce Trent-1000 that is used in the Boeing 787 Dreamline by Air Canada. Two proposed advanced powering systems that are combined with the turbofan are the MCFC-turbofan and SOFC-turbofan. Energy and exergy analyses are conducted to investigate the performance of aircraft at the cruising operation mode. The used fuels are kerosene and an alternative fuel blend of 75% methane and 25% hydrogen. The following conclusions are drawn from the study:

- The fuel mass flow rates are 6 kg/s for kerosene and about 0.017 kg/s for the alternative fuel blend.
- The base turbofan has a maximum thrust force of 153 kN, while the SOFC- and MCFC-turbofans have 116 kN and 107 kN, respectively.
- The thermal efficiencies are 43.4% for the base-turbofan, 52.8% for the SOFC-turbofan, and 71% for the MCFC-turbofan.
- The exergy efficiencies are 52% for the base-turbofan, 66.2% for the SOFC-turbofan, and 87.6% for the MCFC-turbofan.
- The weight of the base-turbofan is 6 tons and increases to 8.2 tons for the SOFC and 11.6 tons for the MCFC.
- The increase in the fuel cell decreases the thrust-to-weight ratio from 2.61 for the base-turbofan to 1.53 for the SOFC-turbofan and 1.06 for the MCFC-turbofan.
- The net power is 47 MW, 33 MW, and 32 MW for the base-turbofan, SOFC-turbofan, and MCFC-turbofan, respectively.
- The combustion chamber produces the highest exergy destruction rates, followed by the hot and fan nozzles.
- The carbon emissions have been reduced from 18 kg/s to about 3.7 kg/s using the alternative fuel blend.
- Increasing the current density of fuel cells decreases the electric efficiency for both fuel cells but increases the weight of the MCFC and decreases the weight of the SOFC.
- Adding a fuel cell increases the engine weight but increases the performance and reduces the emissions.

Further recommendations are to conduct exergoeconomic and

exergoenvironmental analyses on aviation engines to produce a comprehensive understanding of the proposed systems and compare them with traditional engines.

Declaration of competing interest

The authors declare that they have no known competing financial interests or personal relationships that could have appeared to influence the work reported in this paper.

Acknowledgement

The financial support provided by the Natural Sciences and Engineering Research Council of Canada (NSERC) is gratefully acknowledged. The authors also acknowledge the financial support provided by the Transport Canada through its Clean Transportation Program-Research and Development.

Credit author statement

Shaimaa Seyam: Methodology, Software, date curation, Writing – original draft preparation, Investigation, Visualization, editing, Ibrahim Dincer: Supervision, Conceptualization, Funding acquisition, writing-reviewing, and editing, Martin Agelin-Chaab: Supervision, Conceptualization, and Funding acquisition, writing-reviewing, and editing.

References

[1] Lee DS, Fahey DW, Skowron A, Allen MR, Burkhardt U, Chen Q, et al. The contribution of global aviation to anthropogenic climate forcing for 2000 to 2018. Atmos Environ 2021:244. https://doi.org/10.1016/j.atmosenv.2020.117834.
[2] Natural Resources Canada. Transportation sector – energy use analysis | natural resources Canada. Nat Resour Canada; 2019. https://oee.nrcan.gc.ca/corporate/statistics/neud/dpa/showTable.cfm?type=AN&sector=tran&juris=00&rn=1&page=0. [Accessed 14 January 2021].
[3] Natural Resources Canada. Energy fact book 2020-2021. Natural Resources Canada; 2020.
[4] Government of Canada. Canada's Action Plan to reduce greenhouse gas emissions from aviation. Government of Canada; 2019.
[5] Kousoulidou M, Lonza L. Biofuels in aviation: fuel demand and CO2 emissions evolution in Europe toward 2030. Transport Res Transport Environ 2016;46:166–81. https://doi.org/10.1016/j.trd.2016.03.018.
[6] Schripp T, Grein T, Zinsmeister J, Oßwald P, Köhler M, Müller-Langer F, et al. Technical application of a ternary alternative jet fuel blend – chemical characterization and impact on jet engine particle emission. Fuel 2021;288. https://doi.org/10.1016/j.fuel.2020.119606.
[7] Luo F, Song W, Chen W, Long Y. Investigation of kerosene supersonic combustion performance with hydrogen addition and fuel additive at low Mach inflow conditions. Fuel 2021;285:119139. https://doi.org/10.1016/j.fuel.2020.119139.
[8] Badami M, Nuccio P, Pastrone D, Signoretto A. Performance of a small-scale turbojet engine fed with traditional and alternative fuels. Energy Convers Manag 2014;82:219–28. https://doi.org/10.1016/j.enconman.2014.03.026.
[9] Petrescu RVV, Machín A, Fontánez K, Arango JC, Márquez FM, Petrescu FIT. Hydrogen for aircraft power and propulsion. Int J Hydrogen Energy 2020;45:20740–64. https://doi.org/10.1016/j.ijhydene.2020.05.253.
[10] Valera-Medina A, Morris S, Runyon J, Pugh DG, Marsh R, Beasley P, et al. Ammonia, methane and hydrogen for gas turbines. Energy Procedia 2015;75:118–23. https://doi.org/10.1016/j.egypro.2015.07.205.
[11] Bicer Y, Dincer I. Life cycle evaluation of hydrogen and other potential fuels for aircrafts. Int J Hydrogen Energy 2017;42:10722–38. https://doi.org/10.1016/j.ijhydene.2016.12.119.
[12] Liu X, Reddi K, Elgowainy A, Lohse-Busch H, Wang M, Rustagi N. Comparison of well-to-wheels energy use and emissions of a hydrogen fuel cell electric vehicle relative to a conventional gasoline-powered internal combustion engine vehicle. Int J Hydrogen Energy 2019;45:972–83. https://doi.org/10.1016/J.IJHYDENE.2019.10.192.
[13] Ahmadi P, Torabi SH, Afsaneh H, Sadegheih Y, Ganjehsarabi H, Ashjaee M. The effects of driving patterns and PEM fuel cell degradation on the lifecycle assessment of hydrogen fuel cell vehicles. Int J Hydrogen Energy 2019:1–14. https://doi.org/10.1016/j.ijhydene.2019.01.165.
[14] Ji Z, Qin J, Cheng K, Liu H, Zhang S, Dong P. Performance evaluation of a turbojet engine integrated with interstage turbine burner and solid oxide fuel cell. Energy 2019;168:702–11. https://doi.org/10.1016/j.energy.2018.11.088.
[15] Waters DF, Cadou CP. Engine-integrated solid oxide fuel cells for efficient electrical power generation on aircraft. J Power Sources 2015;284:588–605. https://doi.org/10.1016/j.jpowsour.2015.02.108.
[16] Ji Z, Qin J, Cheng K, Dang C, Zhang S, Dong P. Thermodynamic performance evaluation of a turbine-less jet engine integrated with solid oxide fuel cells for unmanned aerial vehicles. Appl Therm Eng 2019;160:114093. https://doi.org/10.1016/j.applthermaleng.2019.114093.
[17] Bakalis DP, Stamatis AG. Optimization methodology of turbomachines for hybrid SOFC-GT applications. Energy 2014;70:86–94. https://doi.org/10.1016/j.energy.2014.03.093.
[18] Verstraete D. Long range transport aircraft using hydrogen fuel. Int J Hydrogen Energy 2013;38:14824–31. https://doi.org/10.1016/j.ijhydene.2013.09.021.
[19] Canada's climate plan. Canada.ca n.d. https://www.canada.ca/en/services/environment/weather/climatechange/climate-plan.html. [Accessed 30 November 2019].
[20] EASA. Type-certificate data sheet for Trent 1000 series enginesEASA.E.036. Rolls-Royce Deutschland Ltd & Co KG: European Union Aviation Safety Agency; 2019.
[21] Dincer I, Rosen MA. Exergy: energy, environment and sustainable development. second ed. Oxford, UK: Elsevier; 2013.
[22] Kerrebrock JL. Aircraft engines and gas turbines. second ed. Massachusetts, USA: The MIT Press; 2012. https://doi.org/10.1007/978-0-230-35686-3_1.
[23] El-Sayed AF. Aircraft propulsion and gas turbine engines. Florida, US: CRC Press; 2008. https://doi.org/10.1201/9781420008777.
[24] McCarty RD, Hord J, Roder HM. Selected properties of hydrogen (engineering design data). U.S. Department of Commerce/National Bureau of Standards; 1981.
[25] Çengel YA, Boles MA. Thermodynamics: a engineering approach. USA: Eighth. McGraw-Hill Education; 2015. https://doi.org/10.1109/MILCOM.2005.1605829.
[26] Shehata MS, Elkotb MM, Salem H. Combustion characteristics for turbulent prevaporized premixed flame using commercial light diesel and kerosene fuels. J Combust 2014;2014. https://doi.org/10.1155/2014/363465.
[27] Vielstich W, Lamm A, Gasteiger HA. Handbook of fuel cells - fundamentals, technology and applications. John Wiley & Sons, Ltd.; 2010. https://doi.org/10.1002/9780470974001.f500032.
[28] Sundmacher K, Kienle A, Pesch HJ, Berndt JF, Huppmann G. Molten carbonate fuel cells: modeling, analysis, simulation, and control. Verlag, wienheim, Germany. Wiley; 2007. https://doi.org/10.1002/9783527611324.
[29] Ahn J, Park SH, Lee S, Noh Y, Chang D. Molten carbonate fuel cell (MCFC)-based hybrid propulsion systems for a liquefied hydrogen tanker. Int J Hydrogen Energy 2018;43:7525–37. https://doi.org/10.1016/j.ijhydene.2018.03.015.
[30] Koh JH, Kang BS, Lim HC. Analysis of temperature and pressure fields in molten carbonate fuel cell stacks. AIChE J 2001;47:1941–56. https://doi.org/10.1002/aic.690470906.
[31] Lysik A, Wejrzanowski T, Cwieka K, Skibinski J, Milewski J, Marques FMB, et al. Silver coated cathode for molten carbonate fuel cells. Int J Hydrogen Energy 2020;45. https://doi.org/10.1016/j.ijhydene.2020.05.112. 19847–57.
[32] Minutillo M, Perna A, Jannelli E. SOFC and MCFC system level modeling for hybrid plants performance prediction. Int J Hydrogen Energy 2014;39:21688–99. https://doi.org/10.1016/j.ijhydene.2014.09.082.
[33] Bessette NF, Wepfer WJ. A mathematical model of a tubular solid oxide fuel cell. J Energy Resour Technol Trans ASME 1995;117:43–9. https://doi.org/10.1115/1.2835319.
[34] Milewski J, Swirski K, Santarelli M, Leone P. Advanced methods of solid fuel cell modeling. 2011.
[35] Ji Z, Qin J, Cheng K, Guo F, Zhang S, Dong P. Thermodynamics analysis of a turbojet engine integrated with a fuel cell and steam injection for high-speed flight. Energy 2019;185:190–201. https://doi.org/10.1016/j.energy.2019.07.016.
[36] Version 10 Physical property data: reference manual. Aspen Technology Inc.; 1999.
[37] Sandler SI. Using aspen Plus ® in thermodynamics instruction: a step-by-step guide. AICHE - Wiley; 2015.
[38] Peng DY, Robinson DB. A new two-constant equation of state. Ind Eng Chem Fundam 1976;15:59–64. https://doi.org/10.1021/i160057a011.
[39] Whyatt GA, Chick LA. Electrical generation for more-electric aircraft using solid oxide fuel cells. 2012.
[40] Ji Z, Rokni MM, Qin J, Zhang S, Dong P. Energy and configuration management strategy for battery/fuel cell/jet engine hybrid propulsion and power systems on aircraft. Energy Convers Manag 2020;225:113393. https://doi.org/10.1016/j.enconman.2020.113393.